


Article

# Simulation and Measurement of Energetic Performance in Decentralized Regenerative Ventilation Systems

Nicolas Carbonare <sup>1,2,\*</sup>, Hannes Fugmann <sup>1</sup> , Nasir Asadov <sup>1</sup>, Thibault Pflug <sup>1</sup>, Lena Schnabel <sup>1</sup> and Constanze Bongs <sup>1</sup>

<sup>1</sup> Fraunhofer Institute for Solar Energy Systems, Heidenhofstr. 2, 79110 Freiburg, Germany; hannes.fugmann@ise.fraunhofer.de (H.F.); asadov.nasir@gmail.com (N.A.); thibault.pflug@ise.fraunhofer.de (T.P.); lena.schnabel@ise.fraunhofer.de (L.S.); constanze.bongs@ise.fraunhofer.de (C.B.)

<sup>2</sup> Building Science Group, Karlsruhe Institute of Technology, Englerstr. 7, 76131 Karlsruhe, Germany

\* Correspondence: nicolas.carbonare@ise.fraunhofer.de; Tel.: +49-761-4588-2151

Received: 15 October 2020; Accepted: 12 November 2020; Published: 17 November 2020



**Abstract:** Decentralized regenerative mechanical ventilation systems have acquired relevance in recent years for the retrofit of residential buildings. While manufacturers report heat recovery efficiencies over 90%, research has shown that the efficiencies often vary between 60% and 80%. In order to better understand this mismatch, a test facility is designed and constructed for the experimental characterization and validation of regenerative heat exchanger simulation models. A ceramic honeycomb heat exchanger, typical for decentralized regenerative ventilation devices, is measured in this test facility. The experimental data are used to validate two modeling approaches: a one-dimensional model in Modelica and a computational fluid dynamics (CFD) model built in COMSOL Multiphysics<sup>®</sup>. The results show an overall acceptable thermal performance of both models, the 1D model having a much lower simulation time and, thus, being suitable for integration in building performance simulations. A test case is designed, where the importance of an appropriate thermal and hydraulic modeling of decentralized ventilation systems is investigated. Therefore, the device is integrated into a multizone building simulation case. The results show that including component-based heat recovery and fan modeling leads to 30% higher heat losses due to ventilation and 10% more fan energy consumption than when assuming constant air exchange rates with ideal heat recovery. These findings contribute to a better understanding of the behavior of a growing technology such as decentralized ventilation and confirm the need for further research on these systems.

**Keywords:** decentralized ventilation; heat recovery; honeycomb heat exchanger; computational fluid dynamics; Modelica

## 1. Introduction

Residential building retrofitting occurs in Germany at a pace of 1% yearly and should be increased to 3% in the coming years to reach the desired energy targets [1]. Higher energy efficiency standards for residential buildings are typically associated with more airtight dwellings. Residential indoor air quality and health improve only when building retrofitting is accompanied by an appropriate residential ventilation commissioning [2]. In that sense, decentralized regenerative ventilation systems (DRVSs) (Figure 1) have been gaining popularity on the market for several years already [3], due to their simplicity of installation and low price.



**Figure 1.** Component arrangements of a typical decentralized regenerative ventilation device (1—inner wall aperture, 2—fan, 3—heat exchanger, 4—outer wall aperture) [4].

The most common material used for heat exchangers is ceramics. However, models utilizing aluminum for this purpose can also be found on the market. The reversible fans are usually of an axial flow type and operate at relatively low noise levels. The maximum flow rates provided by the devices are around 40 m<sup>3</sup>/h on average. The typical cycle period is about two minutes (one minute of exhaust air extraction and one minute of fresh air supply).

Although research has mostly focused on centralized ventilation systems and air handling units, some publications analyze DRVSs and their different characteristics. Angsten et al. [5] highlighted the costs, installation process simplicity, and room-individual control as the key advantages of DRVSs. On the other side, they reported that the ventilation effectiveness can be severely affected by a strong pressure difference between the façade and the room. This was confirmed later by Mikola et al. [6], who studied the hydraulic performance of these devices under different pressure configurations but assuming a heat recovery profile depending on the volume flow. Baldini et al. [7] reported that with appropriate control strategies, wind loading could be used to provide fan energy savings of up to 76% in DRVSs, taking advantage of the above-mentioned differential pressure. Undesired volume flows can cause a draft. Mahler et al. [8] reported draft issues in 30% of the analyzed buildings. This is directly associated with the thermal performance of the heat recovery system (too low supply temperatures). Correct modeling of the heat recovery system becomes crucial for the thermohydraulic performance of DRVSs. Merzkirch et al. [9] reported heat recovery efficiencies in DRVSs to be from 68% to 76% in laboratory experiments. Besides, increasing the pressure difference between the room and the outdoor environment can lead to up to 150% volume flow deviations from the nominal value. Coydon et al. [10] developed a model to calculate the heat recovery efficiency of DRVSs, taking into account the energy balance of the room as well. Extending his method to building performance simulation, heat recovery efficiencies of around 70% were reported. Smith et al. [11] simulated the performance of DRVSs in residences using a moisture-based demand-controlled ventilation scheme. Moisture recovery was observed in these devices, leading to a poor air quality performance of DRVSs in humid rooms (such as the bathroom). Temperature-based heat recovery efficiencies between 70% and 90% were reported. Manz et al. [12] studied the heat recovery, ventilation efficiency, and acoustic performance of DRVSs. He concluded that high sound pressure levels in these devices can lead to high user dissatisfaction. Recently, the proper hydraulic modeling of the alternating behavior of the fans has been defined as one of the priorities in DRVSs [13].

Regenerators were also researched in recent years, although rarely connected to DRVSs. Muralikrishna [14] successfully modeled the heat transfer between air and a counterflow metallic regenerator using different thermal models. Liu et al. [15] modeled the forced convection heat transfer in metal honeycomb heat exchangers, using the two-equation method. They reported that metal honeycombs with a high cell-wall length are advantageous for optimizing the thermal performance with a lower pressure drop. Mesonero et al. [16] modeled the heat storage process of a fixed-bed regenerator in a solar-powered combined cycle and validated the model with laboratory

measurements. Gateau et al. [17] compared honeycomb and fin heat exchangers using computational fluid dynamics (CFD). According to the results, radiation heat transfer represents only around 3% of the total heat exchanged, being dominated by convection. Li et al. [18] investigated the heat transfer between airflow and a honeycomb ceramic air receiver. The heat transfer was more sensitive to the airflow characteristics than the honeycomb properties. The authors also studied the sensitivity of the thermal efficiency to the variation of the regenerator shape. The thermal mass of the regenerator correlated positively to the thermal efficiency (influenced by wall thickness, channel width, or channel length).

Overall, the literature review confirmed that DRVS solutions are rapidly gaining market, especially in the renovation of residential buildings, and that there are increasing efforts to solve the acknowledged drawbacks of these devices. Information on their performance is limited, and different publications report a wide range of heat recovery efficiencies (50% to 90%), given the lack of a single evaluation method for heat recovery systems [19]. This study aims to precisely model the thermal effects in these devices to reduce the gap between predicted and measured energy consumption in residential buildings. A complex (CFD) and a simplified (1D) model are developed and compared with laboratory measurements to validate the thermal performance of regenerative heat recovery systems. The DRVS simplified model is later applied in a case study to analyze the impact of pressure difference and wind loads on their performance, the air exchange rate, and the simulated heat recovery. This publication addresses the importance of modeling pressure differences in the façade and room, the relevance of advanced modeling of heat recovery systems in DRVS, and their impact on the indoor environmental quality in a building simulation.

## 2. Methodology

In this publication, we propose an analysis regarding regenerative heat exchangers for decentralized ventilation systems. Two different modeling approaches are compared and validated through laboratory measurements of a ceramic honeycomb regenerative heat exchanger. This device is usually found in DRVSs, as mentioned before. The first modeling approach is carried out using computational fluid dynamics. Therewith, the time-dependent temperature, velocity, and pressure fields are solved numerically for a three-dimensional symmetric segment of the heat exchanger with the finite element method (FEM) using the software Comsol Multiphysics®. The second approach is performed using a simplified 1D model in Modelica. The discretization level of this model is lower than the one using CFD. A priori, the CFD model leads to a better representation of the thermal behavior of the regenerator. Modelica 1D models are already proven to properly represent different fluid systems and components with a simplified modeling approach. This procedure is suitable for coupling with other building simulation models [20]. A parametric analysis is carried out, varying the fan speed and the cycle length of the fan. The simplified approach can provide a reasonable solution to be integrated into building performance simulation when the focus is on the ventilation system and not the regenerator. Both models are compared with measurements carried out in a test facility. Finally, the simplified model is applied in a case study of a building simulation to quantify the importance of proper DRVS modeling rather than assuming a constant efficiency.

### 2.1. Heat Exchanger

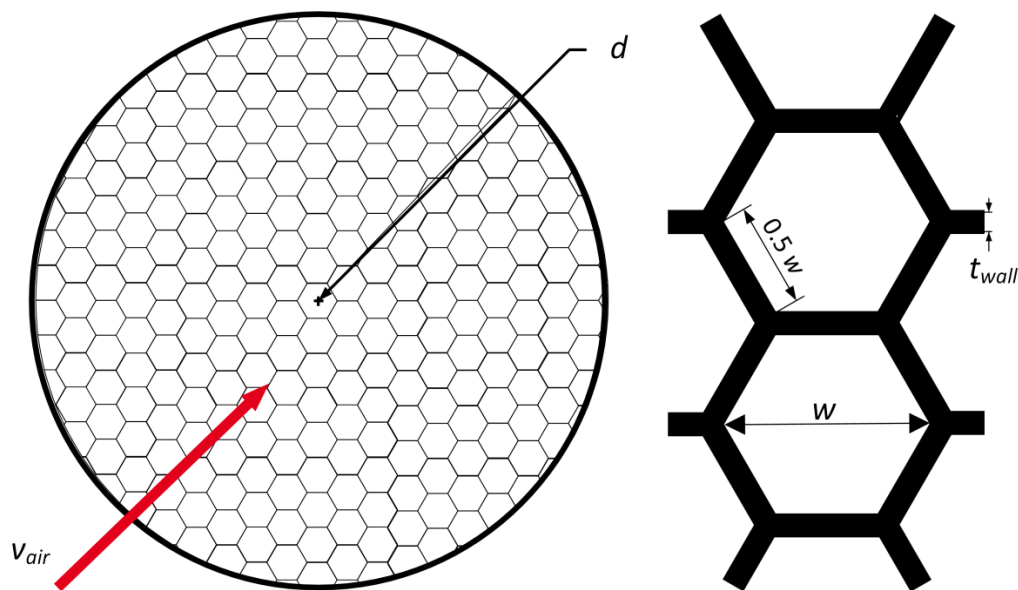
The heat recovery system consists of a cylindrical regenerator with honeycomb-shaped channels. The properties of the heat exchanger are summarized in Table 1. The thermal properties are provided by the manufacturer, resulting in an average heat recovery efficiency of 81% [4].

The free flow area is defined as the cross-sectional area of one hexagonal channel (without the wall) multiplied by the number of channels. Figure 2 shows the geometry of cylindrical heat exchangers.

As mentioned before, DRVSs change their direction periodically, allowing the regenerator to store and release heat between phases. In Table 2, the values for the parametric analysis of the regenerator are listed.

**Table 1.** Honeycomb heat exchanger properties with hexagonal shape.

Variable	Unit	Value
Channel width $w$	m	0.004
Channel length $l$	m	0.15
Channel area $A_{\text{chan}}$	m <sup>2</sup>	$4.16 \times 10^{-5}$
Cylinder diameter $d$	m	0.142
Free flow area $A_{\text{flow}}$	m <sup>2</sup>	0.0104
Mass	kg	2.32
Specific heat capacity $c_{p,\text{solid}}$	J kg <sup>-1</sup> K <sup>-1</sup>	877
Density $\rho_{\text{solid}}$	kg m <sup>-3</sup>	2700
Thermal conductivity $k_{\text{solid}}$	W m <sup>-1</sup> K <sup>-1</sup>	0.026
Number of channels $n_{\text{chan}}$	-	1000
Wall thickness $t_{\text{wall}}$	m	0.001

**Figure 2.** Scheme of the honeycomb ceramic regenerator; front view (left) and channel model (right).**Table 2.** List of parametric values. The used characteristic length to calculate the Reynolds number is the hydraulic diameter  $d_h$ , defined in Equation (15).

Cycle Length	Fan Speed	Channel Mean Air Velocity $v_{\text{air}}$ (m.s <sup>-1</sup> )	Reynolds Number $Re$ (-)
60 s	50%	0.40	92
	100%	0.89	204
180 s	50%	0.40	92
	100%	0.89	204

## 2.2. Laboratory Test Facility

Within the scope of this study, a specific test facility was built for the characterization of heat exchanger structures in decentralized regenerative ventilation devices. Figure 3 shows the main parts of the test facility.

Unlike for the testing procedures in climate chambers, where both a hot and a cold ambient temperature are present, in the suggested test facility design, only the “room” exists (Figure 3: Room Air Provision). The room temperature was approximately 18 °C with a relative humidity of approximately 30%. The outside ambient temperature was simulated by guiding conditioned air at a low flow rate through a duct with a diameter of 150 mm along the inlet of the test facility

(Figure 3: Ambient Air Provision). The ambient air had a temperature of approximately 8 °C at a relative humidity of 37%. These conditions on both sides of the device were constantly measured. In the supply case, the fan will suck the conditioned air through the heat exchanger. Temperature, differential pressure, and humidity sensors were carefully selected to be able to obtain a high enough measurement resolution for trustworthy assessment, before and after the heat exchanger (see Table 3 for details). Four temperature sensors were shifted 90° between each other to capture the temperature of the whole air profile. The supply air leaves the heat exchanger, enters a mass flow sensor, and leaves the test facility into the room. In the exhaust phase, when the fan reverses the flow direction in the test facility, the exhaust air first enters the mass flow sensor area, then the fan, and then the heat exchanger. Problems related to mixing of the ambient air and the thermal mass of the steel ducts arose, thereafter, in the ambient area. For this reason, the exhaust air was pushed back into the room through another duct. To switch between the above-mentioned flow patterns, a control strategy utilizing two motorized dampers was used (Figure 3: Air Dampers).

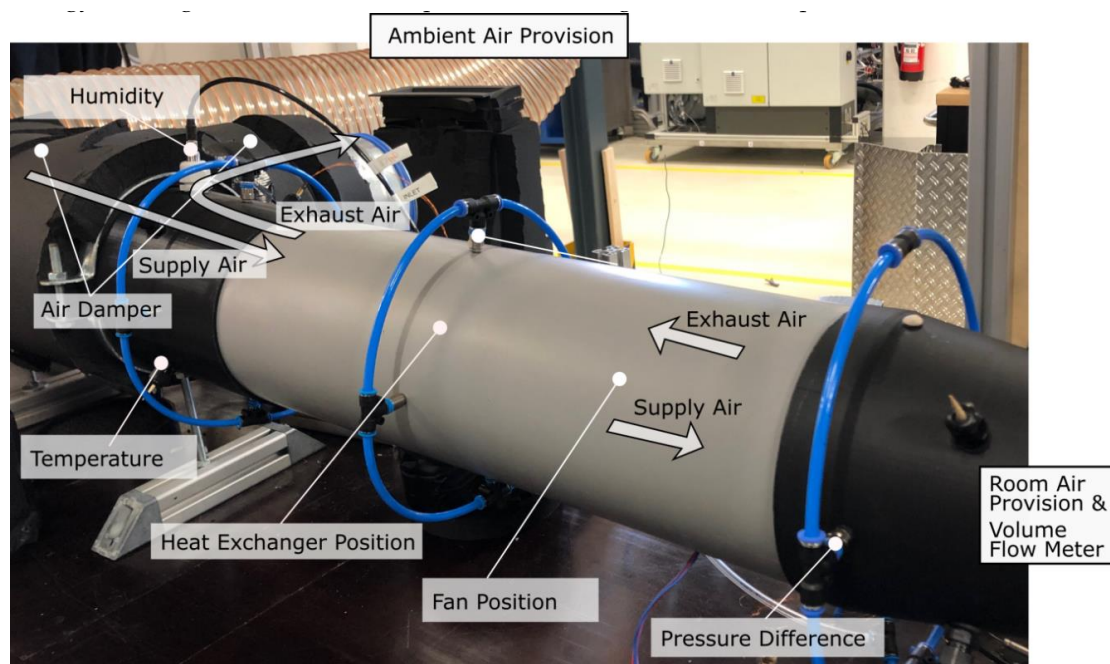


Figure 3. Test facility without insulation.

Table 3. Uncertainties of main sensors.

Sensor	Model	Range	Accuracy	Response Time
Temperature	IST RTD Platinum	−50–+150 °C	±0.1 K (after calibration)	$\tau_{0.63} = 1200 \text{ ms}$ ( $v_{\text{air}} = 1 \text{ m/s}$ )
Humidity	Vaisala HMT 120	0–100% rH	±1.5% rH	
Differential pressure	h-w PU ± 50	−50–+50 Pa	±0.5% m.v.	20 ms
Mass flow rate	E+H B200 Prosonic Flow	0–300 m <sup>3</sup> .h <sup>1</sup>	±1.5% m.v.	$\tau_{0.95} = 1000 \text{ ms}$

During the supply phase, one damper is open and the other damper is closed, which leads to the conditioned air being sucked freely from the ambient air output. The damper position states invert as soon as the exhaust phase starts. Here, the opening/closing speed of the damper plays a big role in avoiding the mixing of supply and exhaust air, which have different temperatures and humidity. For this purpose, the fastest running actuators available for the given application were selected. Their running time of just 2.5 s is lower than the time that the fan impeller needs to stop from an average rotational speed and to start spinning with the same revolutions per minute (RPM) in the reverse direction, facilitating an articulate transition between supply and exhaust phases.

As the temperatures were measured at the inlet and outlet of the device, the values should be corrected to assess the performance of the heat exchanger as storage alone. Therefore, anything that boosts or hinders (depending on whether it is a supply or an exhaust phase) the efficiency of the device compared to the efficiency of the storage alone was quantified. In this study, the total gains  $\dot{Q}_{\text{gains}}$  were assumed to be equal to the sum of the heat, infiltrating the housing of the device ( $\dot{Q}_{\text{inf}}$ ) as well as the waste heat generated by the fan ( $\dot{Q}_{\text{fan}}$ ). The total gains  $\dot{Q}_{\text{gains}}$  were estimated by measuring their effect on the air temperature profile and represent around 5% of the total heat transferred between air and heat storage ( $\dot{Q}_{\text{sup}} - \dot{Q}_{\text{exh}}$ ). Thus, it holds that:

$$\dot{Q}_{\text{gains}} = \dot{Q}_{\text{fan}} + \dot{Q}_{\text{inf}} \quad (1)$$

Thermal infiltrations on the left-hand side of the heat exchanger are significantly higher than on the right-hand side (left and right according to Figure 4). This happens because the left-hand side is the “inlet” of the supply side (ambient) and therefore always has lower temperatures than the device, causing a higher thermal infiltration. For this reason, infiltrations were assumed to happen on this side and were, thus, neglected on the right side.

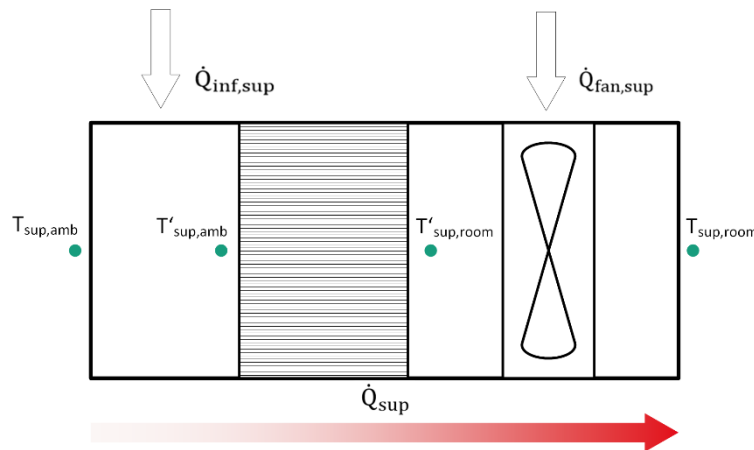


**Figure 4.** Gains in the flow temperature on the supply phase ( $T_{\text{sup,amb}}$  and  $T_{\text{sup,room}}$  are temperatures on the ambient and the room side of the device, respectively, where the temperature sensors were placed).

The effect of  $\dot{Q}_{\text{fan}}$  was estimated for both phases according to the temperature gradient that it causes in the flow. The effects of varying total efficiency of the fan ( $\eta_e$ ) could not be considered, as the electrical input power to the fan was not measured. Therefore, the inlet and outlet temperatures were corrected as follows:

$$T'_{\text{sup,amb}} = T_{\text{sup,amb}} + \frac{\dot{Q}_{\text{inf,sup}}}{\dot{m}_{\text{sup}}c_{p,\text{air}}} \quad (2)$$

$$T'_{\text{sup,room}} = T_{\text{sup,room}} - \frac{\dot{Q}_{\text{fan,sup}}}{\dot{m}_{\text{sup}}c_{p,\text{air}}} \quad (3)$$

$$T'_{\text{exh,amb}} = T_{\text{exh,amb}} + \frac{\dot{Q}_{\text{fan,exh}}}{\dot{m}_{\text{exh}}c_{p,\text{air}}} \quad (4)$$

$$T'_{\text{exh,room}} = T_{\text{exh,room}} - \frac{\dot{Q}_{\text{inf,exh}}}{\dot{m}_{\text{exh}}c_{p,\text{air}}} \quad (5)$$

The corrected temperatures will be used for the model validation. One exemplary temperature curve is shown in Figure 5. The curves show a slow progression of the temperature on both sides so

that an equilibrium state with constant temperatures is never reached. The small sudden decrease in the temperature in the phase transition is due to the temperature correction previously described (where the fan direction change occurs).

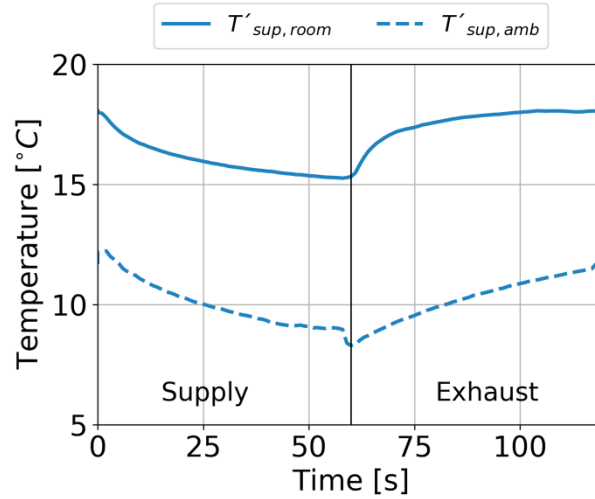


Figure 5. Exemplarily temperature curves of  $T'_{sup,amb}$  and  $T'_{sup,room}$ .

The time-dependent heat transfer rates within the heat exchanger are defined as

$$\dot{Q}_{sup}(t) = \dot{m}_{air} c_{p,air} (T'_{sup,room} - T'_{sup,amb}) \quad (6)$$

$$\dot{Q}_{exh}(t) = \dot{m}_{air} c_{p,air} (T'_{exh,room} - T'_{exh,amb}) \quad (7)$$

where all parameters on the right side are time-dependent as well. The velocities and phase length of the measurement are as according to Table 2. The values of the humidity, temperature, and mass flow rate measurements are used to calculate the mass flow rate  $\dot{m}_{air}$  and the specific heat capacity  $c_{p,air}$ . To be able to quantify the performance of the regenerative device, a characteristic cycle has to be defined. We define this as a cycle with the same starting and ending properties. This cycle will be further referred to as the cycle in “quasi-steady state”. In order to reach this state, each measurement point defined in Table 2 was iterated ten times. The last complete cycle was used for data evaluation. Figure 6 illustrates the workflow of the process, from the transient measurements to the heat recovery supplied. Here, the chosen cycles are indicated between the vertical red dashed lines. The heat supplied is obtained by integrating, over time (supply or exhaust phase), the instantaneous heat transfer rate.

$$Q_{sup} = \int \dot{Q}_{sup}(t) dt = \int \dot{m}_{air} c_{p,air} (T'_{sup,room} - T'_{sup,amb}) dt \quad (8)$$

The heat  $Q_{sup}$  and  $Q_{exh}$  should be equal due to the correction in Equations (6) and (7), with the heat losses and gains taken into account in Equation (1). Thus,  $Q_{sup}$  and  $Q_{exh}$  express the stored energy only. Based on the temperature and flow rate measurements, the values of heat  $Q_{sup}$  and  $Q_{exh}$  show a good accordance, with relative differences of less than 6%. More information about these measurements can be found in the thesis of Asadov [21].

### 2.3. Thermal Model

#### 2.3.1. Finite Element Method for CFD

Time-dependent weakly compressible fluid flow and heat transfer was simulated with COMSOL Multiphysics® (Version 5.5), using the finite element method (FEM). The governing equations for the air/solid domains are the three-dimensional Navier–Stokes equations, which were simplified by

assuming laminar, weakly compressible flow of the Newtonian fluid air with temperature-dependent fluid properties and constant solid properties and neglecting volumetric forces and radiation heat transfer. The continuity, Navier–Stokes, and energy (heat) equations describe the system on the air side:

$$\frac{\partial \rho_{\text{air}}}{\partial t} + \nabla \cdot (\rho_{\text{air}} \mathbf{u}) = 0 \tag{9}$$

$$\rho_{\text{air}} \frac{\partial \mathbf{u}}{\partial t} + \rho_{\text{air}} (\mathbf{u} \cdot \nabla) \mathbf{u} = \nabla \cdot \left[ -p \mathbf{I} + \mu_{\text{air}} (\nabla \mathbf{u} + (\nabla \mathbf{u})^T) - \frac{2}{3} \mu_{\text{air}} (\nabla \cdot \mathbf{u}) \mathbf{I} \right] \tag{10}$$

$$\rho_{\text{air}} c_{p,\text{air}} \mathbf{u} \cdot \nabla T = \nabla \cdot (k_{\text{air}} \nabla T) \tag{11}$$

The air properties  $\rho_{\text{air}}$ ,  $\mu_{\text{air}}$ ,  $c_{p,\text{air}}$ , and  $k_{\text{air}}$  are the density, dynamic viscosity, heat capacity at constant pressure, and thermal conductivity of air, respectively. Their values are a function of the temperature  $T$  and are evaluated at a fixed pressure of 1 atm. The vector  $\mathbf{I}$  is the identity. The scalars for temperature  $T$ , pressure  $p$ , and the velocity field  $\mathbf{u} = (u, v, w)$  are the dependent variables. The viscous dissipation and the work related to thermal expansion are neglected in the energy Equation (11). The energy (heat) equation on the solid side is as follows:

$$\rho_{\text{solid}} c_{p,\text{solid}} \frac{\partial T}{\partial t} = \nabla \cdot (k_{\text{solid}} \nabla T) \tag{12}$$

The properties  $\rho_{\text{solid}}$ ,  $c_{p,\text{solid}}$ , and  $k_{\text{solid}}$  are the density, heat capacity at constant pressure, and thermal conductivity of the solid, respectively, and their values are fixed (Table 1). The heat exchanger geometry consists of repetitive elements. By properties of symmetry, a characteristic element can be specified. This element is shown in Figure 7 in detail. The characteristic element is determined by the wall thickness  $t_{\text{wall}}$ , the channel width  $w$ , and the total length of the channel  $l$ . The air velocity field is determined by inlet velocity  $v_{\text{air,in}}$  and the inlet temperature  $T_{\text{air,in}}$  upstream of the heat exchanger. The boundary conditions for the temperature, pressure, and velocity for the time-dependent weakly compressible laminar flow are shown for the specific heat exchanger in Figure 7 and Table 4.

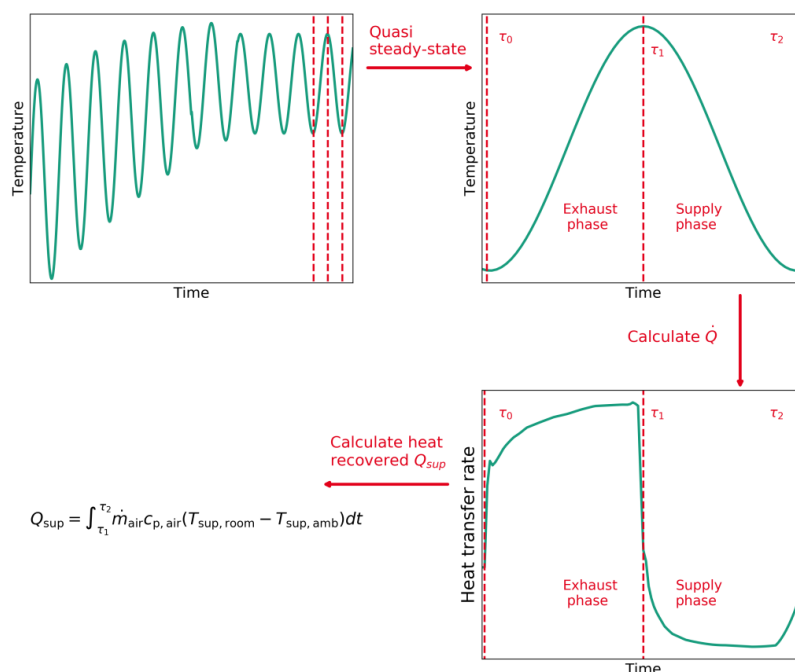
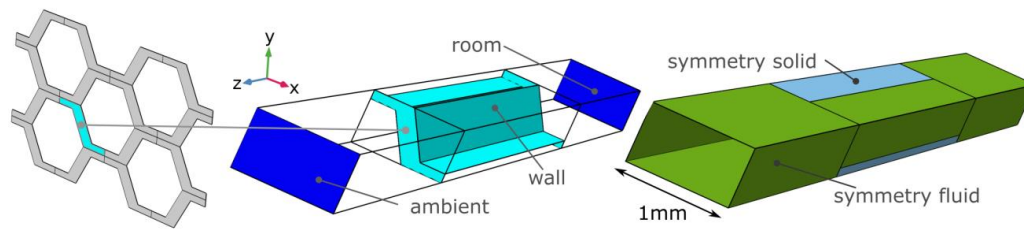


Figure 6. Workflow to calculate the supply heat recovered.





**Figure 7.** Boundary conditions and geometry parameters of the 3D model.

**Table 4.** Boundary conditions; the normal  $\mathbf{n}$  is outward-pointing. The auxiliary matrix variable  $\mathbf{K}$  is defined as  $\mathbf{K} = \mu_{\text{air}}(\nabla\mathbf{u} + (\nabla\mathbf{u})^T) - \frac{2}{3}\mu_{\text{air}}(\nabla\cdot\mathbf{u})\mathbf{I}$ .

Boundary	Velocity $\mathbf{u}=(u,v,w)$ and Pressure $p$	Temperature $T$	Comment
Ambient face	$\mathbf{u} = v_{\text{air,in}} \mathbf{n}$	Supply phase: $T = T_{\text{air,in}}$ exhaust phase: $-k_{\text{air}}\nabla T \cdot \mathbf{n} = 0$	Supply phase: $v_{\text{air,in}} > 0$ exhaust phase: $v_{\text{air,in}} < 0$
Room face	$[-p\mathbf{I} + \mathbf{K}]\mathbf{n} = -p_0\mathbf{n}$	Supply phase: $-k_{\text{air}}\nabla T \cdot \mathbf{n} = 0$ exhaust phase: $T = T_{\text{air,in}}$	$p_0 = 0$ atm, $p_{\text{ref}} = 1$ atm $p_A = p + p_{\text{ref}}$ (abs. pressure) Tangential stress component is set to zero
Symmetry fluid	$\mathbf{u} \cdot \mathbf{n} = 0;$ $[-p\mathbf{I} + \mathbf{K}]\mathbf{n} = \mathbf{0}$	$-k_{\text{air}}\nabla T \cdot \mathbf{n} = 0$	No penetration and vanishing shear stresses
Symmetry solid	–	$-k_{\text{solid}}\nabla T \cdot \mathbf{n} = 0$	–
Wall	$\mathbf{u} =$	–	No slip condition

The governing Equations (9)–(12) were discretized by means of a tetrahedral mesh. The mesh was refined in order to obtain a mesh-independent solution. The Richardson method [22] was used to determine the order of accuracy of the refinement. The normalized grid spacing was based on the mean volume of a tetrahedral element. Exemplarily, three meshes are shown in Figure 8. The mean volume of one element differed from  $9 \times 10^{-3} \text{ mm}^3$  (coarse mesh) to  $1 \times 10^{-3} \text{ mm}^3$  (fine mesh). The mesh refinement was chosen such that the grid convergence indices (GCI) [22] for the mean pressure drop  $\Delta p_{\text{mean}}$  and the mean heat transfer rate  $\dot{Q}_{\text{mean}}$  were below 2.5% for several operating conditions. Thus, the uncertainty due to discretization is expected to be lower than 2.5% for the used “normal” grid. The implicit backward differentiation formula (BDF) solver was used as a time-dependent solver within the simulation. BDFs with an order of accuracy varying from one to two were used with a maximum time stepping of 1 s.

The parametric analysis is based on the temperature and velocity input from the measurement. Analogously to the measurement procedure, 10 cycles were performed consecutively for each parametric step in Table 2. The temperatures of the last cycle have been used to calculate the heat transfer rates for each time step (each second) and, finally, the transferred energy within the cycle (cf. Figure 6).

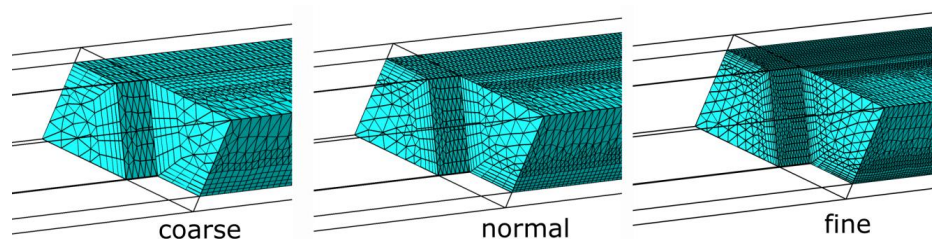


**Figure 8.** Mesh of the heat exchanger. The normal mesh is used for the parametric analysis.

### 2.3.2. Dynamic 1D Model Using Modelica

The heat exchange between the air and the heat recovery system (HRC) could be firstly modeled as a pure convection case. The radiative heat exchange between surfaces is negligible in comparison to the forced convection of the incoming air and the surface of the HRC (honeycomb channels); the temperature rise due to radiation falls under 3% [17]. Equation (13) was obtained applying the first law of thermodynamics in a control volume of the heat exchanger:

$$\dot{Q}(t) = \dot{m}_{\text{air}} c_{p,\text{air}} \frac{\partial T_{\text{air}}}{\partial x} dx = \frac{h_{\text{air}} A_{\text{ht}} dx}{L} (T_{\text{air}} - T_{\text{solid}}) = C_{\text{solid}} \frac{dx}{L} \frac{dT_{\text{solid}}}{dt} \quad (13)$$

where  $\dot{Q}$  is the heat exchange between fluid and the surface of the HRC device;  $\dot{m}_{\text{air}}$  is the mass flow rate of air (kg/s);  $c_{p,\text{air}}$  is the specific heat capacity of air (J/kg K);  $dT$  is the temperature change of the air with time;  $T_{\text{solid}}$  is the temperature on the surface of the solid;  $T_{\text{air}}$  is the air temperature;  $h_{\text{air}}$  is the specific convection coefficient (W/K m<sup>2</sup>);  $C_{\text{solid}}$  is the heat capacity of the solid (KJ/kg);  $A_{\text{ht}}$  is the heat transfer area (contact area between fluid and HRC system); and  $L$  is the heat transfer length.

$$h_{\text{air}} = \frac{Nu k_{\text{air}}}{d_h} \quad (14)$$

where  $Nu$  is the non-dimensional Nusselt number;  $d_h$  is the hydraulic diameter;  $k_{\text{air}}$  is the thermal conductivity of the air. The heat storage on a HRC device was modeled as a capacity that absorbs or releases heat at each time step. The hydraulic diameter  $d_h$  can then be calculated [23]:

$$d_h = \frac{\sqrt{3}}{2} w \quad (15)$$

To calculate the heat transfer at each time step, the Nusselt number must be obtained. The non-dimensional numbers of Reynolds ( $Re$ ) and Prandtl ( $Pr$ ) are used [24]. Since the flow through the channels is laminar ( $Re < 2300$ ), the following correlation to determine the Nusselt number was applied [18].

$$Nu = 3.61 + \frac{0.0668 \left(\frac{d_h}{l}\right) Re Pr}{1 + 0.04 \left[\left(\frac{d_h}{l}\right) Re Pr\right]^{\frac{2}{3}}} \quad (16)$$

Regarding the geometrical modeling approach in Modelica, the heat transfer through the hexagonal channels was modeled as a heat transfer in a pipe (circular tube). The equivalent diameter of this pipe was calculated with the corresponding cross section area during the heat transfer; the equivalent cross-section in the simulated pipe must be the same as in the channels.

$$d_{\text{eq,pipe}} = \sqrt{\frac{3 \sqrt{3} w^2 n_{\text{chan}}}{2 \pi}} \quad (17)$$

Besides, the pipe model was discretized in air flow direction to represent better the temperature progression along with the heat exchanger. Discretization allows a more accurate representation of the heat transfer mechanism, also increasing the computational time. Figure 9 shows the built model in Modelica [25]. The Buildings library [26] supported the modeling process. Each portion of the channel volume was modeled, where the heat transfer between the air (flows between port\_a and port\_b) and honeycomb takes place. Convection heat transfer and heat storage in the honeycomb are also shown.

### 2.4. Fan Hydraulic Model

The fan curve was modeled using the measurement results for the used fan reported in the literature [27]. In this publication, for three different ventilation levels (associated with fan speeds),

a characteristic curve changing the pressure difference between air source and sink was measured. These curves were fitted (quadratic polynomial equation) and used as characteristic curves for the simulation. Since the control strategy used in this simulation study requires four ventilation levels, the corresponding fan speeds and their airflows were interpolated. The resulting curves are depicted in Figure 10.

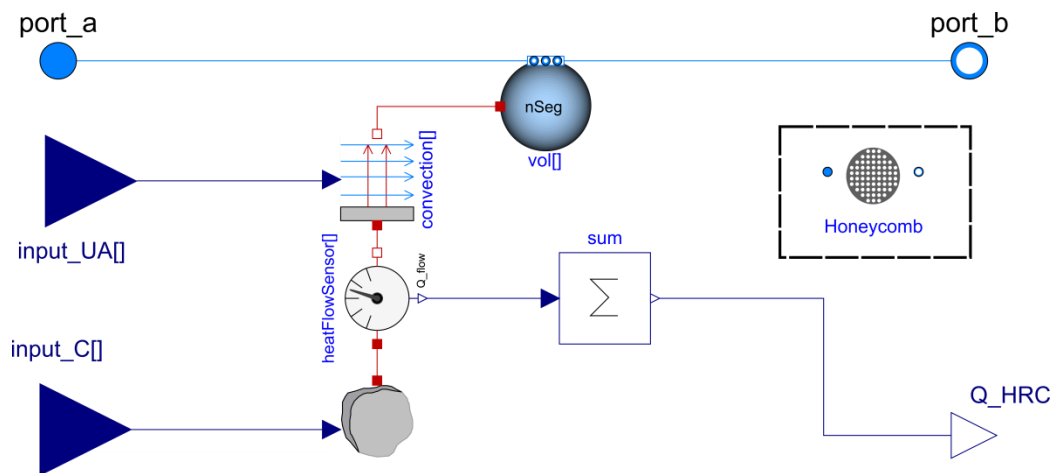


Figure 9. 1D Model in Modelica for the honeycomb heat exchanger.

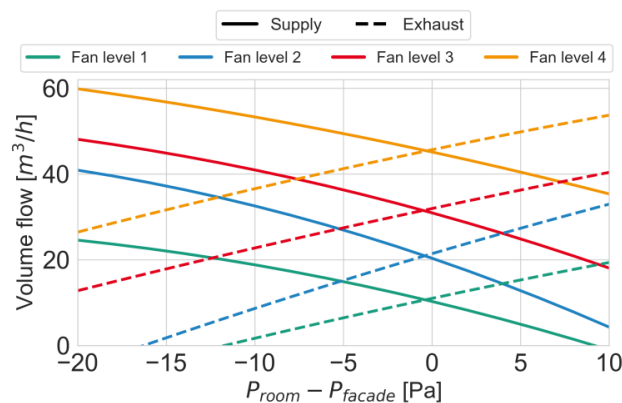


Figure 10. Supply and exhaust airflows given the air speed and pressure difference.

### 2.5. Building Model

A simple building model is used to test the aforementioned ventilation system models within a simulation study in Section 4. A representative apartment of a typical German multifamily building was selected (medium energy retrofit), based on the investigation from the project “LowEx im Bestand” [28]. The floor plan is illustrated in Figure 11.

The building was modeled in EnergyPlus [29], using the airflow network principle [30]. Air movement, infiltration, and wind pressure were simulated by applying this procedure. The pressure on the façade was modeled using the equation of Swami and Chandra [31], which considers both buoyancy and wind-induced pressure. The air movement inside the dwelling was modeled using the power law, and the infiltration using the effective leakage area method. The description and applied coefficients were obtained from the literature [32]. The resulting pressure difference between every room and the outdoor façade influences the airflow rate of the DRVS in the simulation, following the curves in Figure 10.

Regarding the occupant behavior, a time use schedule was taken from the standard ISO 18523-2 [33]. The corresponding loads of heat [34], moisture [35,36], and CO<sub>2</sub> [37] are assigned to the activities from

the time use schedule, which are defined for winter simulations. Other contaminants are not modeled. Window opening behavior was modeled using the probabilistic model from Schweiker et al. [38]. Heating power was modeled ideally, using a defined temperature set point in every room (defined in Table 5 and adapted from the DIN 1946-6 [39]) and keeping the desired temperature with a proportional-integral-derivative (PID) controller.

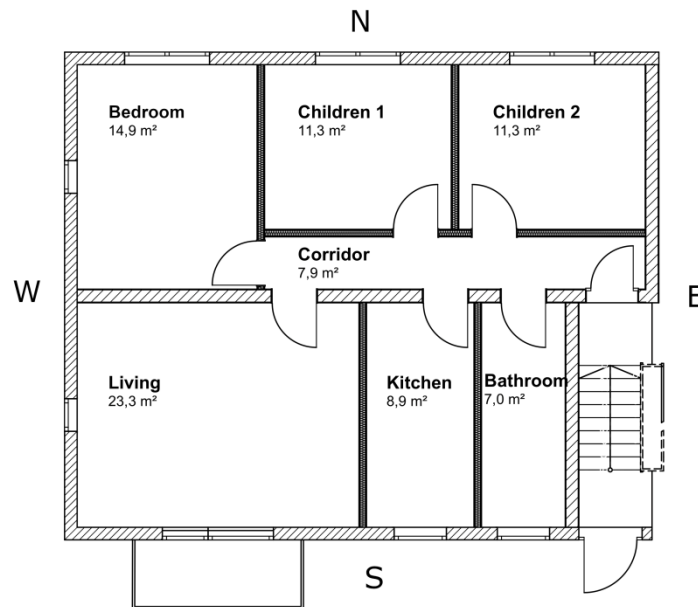


Figure 11. Building floor plan.

Table 5. Room temperature set points (°C). Between brackets, the night setback for the given rooms.

Child 2	Child 1	Bedroom	Living	Kitchen	Bathroom
20(16)	20(16)	20(16)	20	20	22

In every room, one DRVS is installed, except in the bedroom and living room, where two devices are considered. The DRVS is controlled with a stepwise demand-controlled ventilation (DCV) strategy, as shown in Figure 12 [40]. The humid rooms (kitchen and bathroom) are humidity-controlled, and the rest (children, bedroom, and living room) are CO<sub>2</sub>-controlled.

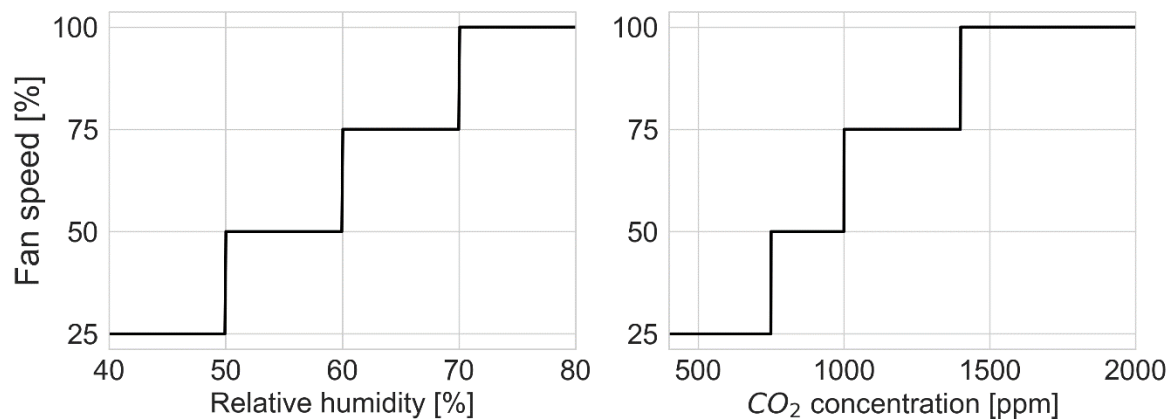


Figure 12. Fan speed in relationship to room relative humidity and CO<sub>2</sub> concentration.

The Modelica and EnergyPlus models were combined in a co-simulation scheme. More details about the models and the simulation set up can be found in the literature [41].

## 2.6. Performance Indicators

The heat recovery efficiency  $\eta_{\text{HRC}}$  is relevant to the performance of DRVS. In this publication, the definition proposed in the DIN EN 308 [42] for the supply side was taken:

$$\eta_{\text{HRC}} = \frac{T_{\text{sup,room}} - T_{\text{amb}}}{T_{\text{room}} - T_{\text{amb}}} \quad (18)$$

The energetic performance of a DRVS is evaluated through the fan energy consumption and heat losses due to ventilation. The corresponding fan power was also measured in the literature [27] for three different ventilation levels. These measurement points are approximated with a quadratic polynomial equation and used to simulate the fan power. The resulting curve is illustrated in Figure 13. The heating energy losses are a function of the ventilation airflow rate, the temperature difference between room and ambient temperatures, and the heat recovery efficiency. This is defined in (19).

$$Q_{\text{heat}} = \int \rho_{\text{air}} \dot{V}_{\text{air}} c_{p,\text{air}} (T_{\text{room}} - T_{\text{amb}}) (1 - \eta_{\text{HRC}}) dt \quad (19)$$

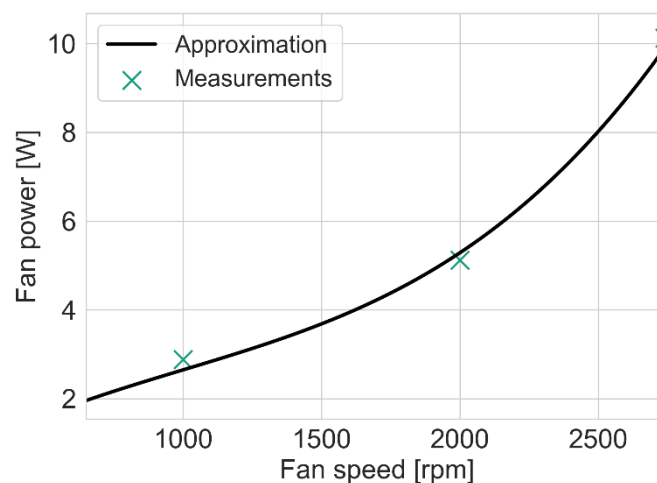


Figure 13. Fan power as a function of the fan speed [27].

In order to properly quantify the differences between simulation models and measurements, two indicators are proposed—the root mean squared error (RMSE) and mean average percentage error (MAPE) [43]. These indicators are defined as follows ( $X$  being a generic variable that was simulated and measured):

$$\text{RMSE} = \sqrt{\frac{\sum_n (X_{\text{sim}} - X_{\text{meas}})_n^2}{n}} \quad (20)$$

$$\text{MAPE} = \frac{\sum_n \left| \frac{X_{\text{sim}} - X_{\text{meas}}}{X_{\text{meas}}} \right|_n}{n} \times 100 \quad (21)$$

These indicators are applied in this work to the supply air temperatures  $T_{\text{sup}}$  to quantify the deviations between simulated and measured values. Since the simulated mass flow rate was the same as the measured one, applying these indicators to the obtained temperatures would be equivalent. These indicators are applied over two periods after the stabilization of the temperatures on both sides

of the heat exchanger. The RMSE has the unit of the measured variable, while the MAPE is expressed in percentage.

### 3. Heat Exchanger Model Validation

#### 3.1. CFD

The resulting heat transfer rates between air and heat storage from the CFD simulation are shown in Figure 14, together with the measured heat exchange for two different fan speeds and a fixed cycle length of 180 s. The heat exchanged was higher in the simulation than in the measurement. Moreover, the shape of the curves is similar in the 50% speed case but shows some differences in the full speed case. In the first 25 s, there is a strong overestimation of the heat exchanged in the CFD simulation (in both phases). This overestimation decays shortly after and, in the end, reaches a similar value to the measurement. The simulated heat exchange has an approximately linear shape after an initial temperature jump at the phase transition between the supply and exhaust phases. Table 6 gives an overview of the simulation results in terms of average heat exchanged  $Q$  and heat recovery efficiency  $\eta_{HRC}$ . The statistical comparison between the CFD simulation, the 1D model, and the measurement is introduced in Section 3.3.

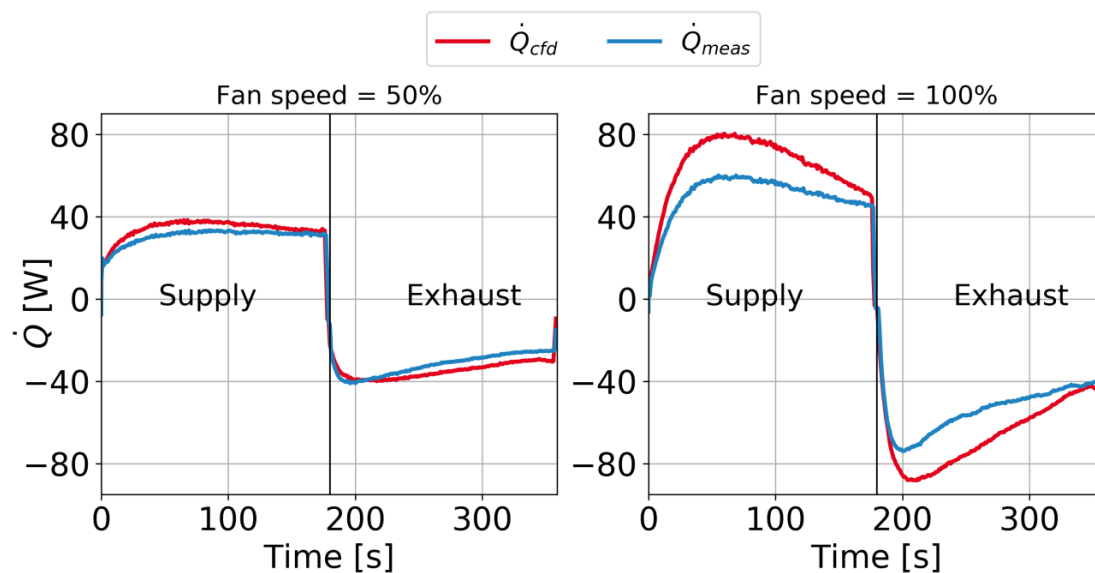


**Figure 14.** Supply and exhaust heat transfer rate comparisons for the measurements and the computational fluid dynamics (CFD) simulation.

**Table 6.** Average heat transfer rate  $\dot{Q}_{cfd}$  on the supply side and heat recovery efficiency  $\eta_{HRC}$  using the CFD model.

Variable	60 s		180 s	
	$\eta_{HRC}$ (-)	$\dot{Q}_{cfd}$ (W)	$\eta_{HRC}$ (-)	$\dot{Q}_{cfd}$ (W)
50% Speed	0.83	30.7	0.80	33.4
100% Speed	0.75	54.5	0.66	63.4

#### 3.2. Modelica 1D Model

In this section, the results of the simulated parametric cases in Modelica are presented. In the first place, a key parameter of the simplified 1D model is the number of nodes of the discretization along the flow direction, and it must be predefined. Figure 15 shows the calculated average RMSE between simulated supply and exhaust temperatures as a function of the number of nodes for the simulation with an alternating period of 60 s and nominal fan speed. The RMSE value stabilizes for models with

six or more nodes. These results were also obtained with other speeds and cycle lengths. Therefore, it was decided that simulations modeling the regenerator with six nodes would be carried out, since a higher number of nodes increased the simulation time but not the performance of the model.

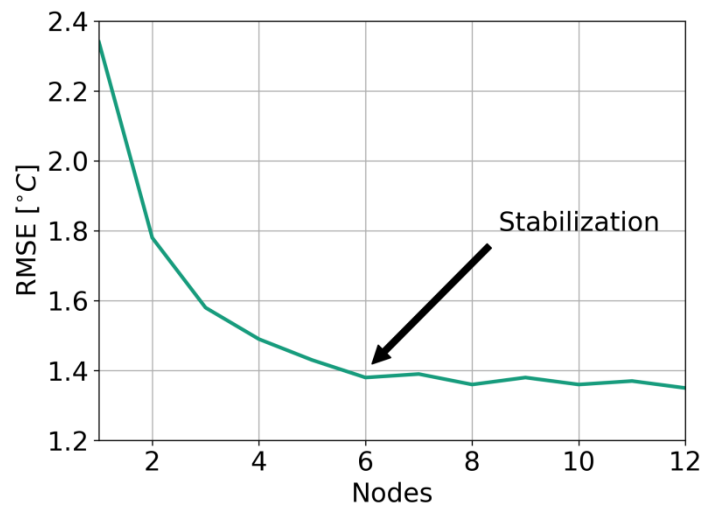


**Figure 15.** Root mean squared error (RMSE) as a function of the number of nodes of the heat storage discretization.

The simulation results for the quasi steady-state cycles of every parametric case are presented in Table 7. As expected, higher air speeds mean a higher heat flux exchanged in both phases. Besides, a higher air speed means a lower heat recovery efficiency, given the higher amount of “hot” air exhausted. This result coincides with the findings of Zemitis et al. [44], who studied the dependency of heat recovery efficiency and pressure difference (and, consequently, the air speed). Considering the cycle period, shorter periods lead to less average heat exchanged but higher efficiencies. The principle is the same as in the analysis of the air speed—a longer cycle means that the regenerator is closer to its heat saturation in both phases, leading to a lower average air supply temperature and, therefore, a lower heat recovery efficiency.

Figure 16 compares the measured and simulated heat transfer rate profiles for the 180-s cycle length. The profiles on both sides of the regenerator in both simulation and measurements show an overall good agreement, although the model overestimates the heat transfer rate at nominal fan speed. The obtained heat transfer rate profiles are in line with the results of Manz et al. [12], who failed to model the temperatures properly during the initial seconds of the direction change. These temperature gaps affect the simulated heat exchange between the airflow and the regenerator. However, the obtained results are satisfactory for the 1D model, and it is suitable for integration into the building performance simulation as it provides a realistic heat recovery efficiency profile.

**Table 7.** Average supply heat transfer rate and heat recovery efficiency using the 1D model and measured values.

Period (s)	60 s				180 s				
	Variable	$\eta_{\text{HRC,1D}}$ (-)	$\eta_{\text{HRC,meas}}$ (-)	$\dot{Q}_{\text{1D}}$ (W)	$\dot{Q}_{\text{meas}}$ (W)	$\eta_{\text{HRC,1D}}$ (-)	$\eta_{\text{HRC,meas}}$ (-)	$\dot{Q}_{\text{1D}}$ (W)	$\dot{Q}_{\text{meas}}$ (W)
50% Speed		0.77	0.80	25.3	27.0	0.76	0.75	30.6	29.9
100% Speed		0.71	0.64	47.6	40.0	0.63	0.54	59.0	49.1

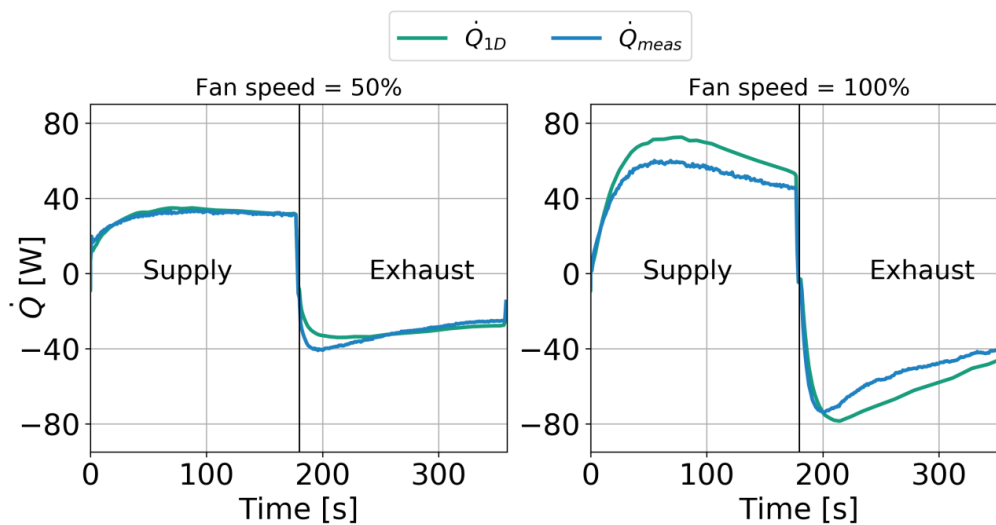


**Figure 16.** Supply and exhaust heat transfer rate comparison for the 180-s cycle length, measured and simulated with 1D Model.

### 3.3. Comparison and Discussion

In this section, the results of the comparison between the test facility measurements and both proposed models are described and discussed. Figure 17 illustrates the supply and exhaust temperature profiles in both phases for 180 s. The initial temperature on both phases shows a slight jump and then a linear behavior. This lies mainly in the direction change of the fan and the inaccurate modeling of the flow, which have already been identified as key factors for the successful representation of DRVSs [13]. This initial difference is emphasized by the temperature correction of the measurements, as described in Section 2.2. Nevertheless, the results confirm that both proposed modeling approaches represent well the thermal behavior of the regenerator.

The 1D model significantly outperformed the CFD model in terms of computational resources. Simulating 3600 s with a 1-s time resolution lasts 0.17 s. On the other hand, the CFD model lasts more than 8 h. Given that CFD models solve the Navier–Stokes equation and energy equation in three dimensions, they can detail the complexity of the airflow inside a channel and take into account several thermal effects in heat transfer. CFD models are an appropriate tool to perform a geometrical optimization of regenerators. The one-dimensional model has many assumptions which do not significantly affect the heat exchanged between the air and the regenerator:

- Dynamic 1D mass and energy balance.
- Discretization in the axial direction (six nodes).
- Neglects radiation.
- Neglects thermal conductivity in heat storage.
- Neglects air velocity profile.

Therefore, the model is suitable for integration into the building performance simulation. Table 8 summarizes the performance indicators for the supply temperatures, proposed in Section 2.6. The CFD model presents absolute deviations between 4% and 10%, while the 1D model is between 1% and 8%. The 1D model presents lower temperature deviations than the CFD model. Given that the 1D model uses correlations from the literature to calculate the Nusselt number, the heat transfer coefficients are based on real measurements. On the other hand, the CFD model obtains the heat transfer coefficients from the calculated flow pattern, the geometry, and material properties, which results, in this case, in a slight overestimation of the heat transfer rate related to both measurements and the Modelica model.



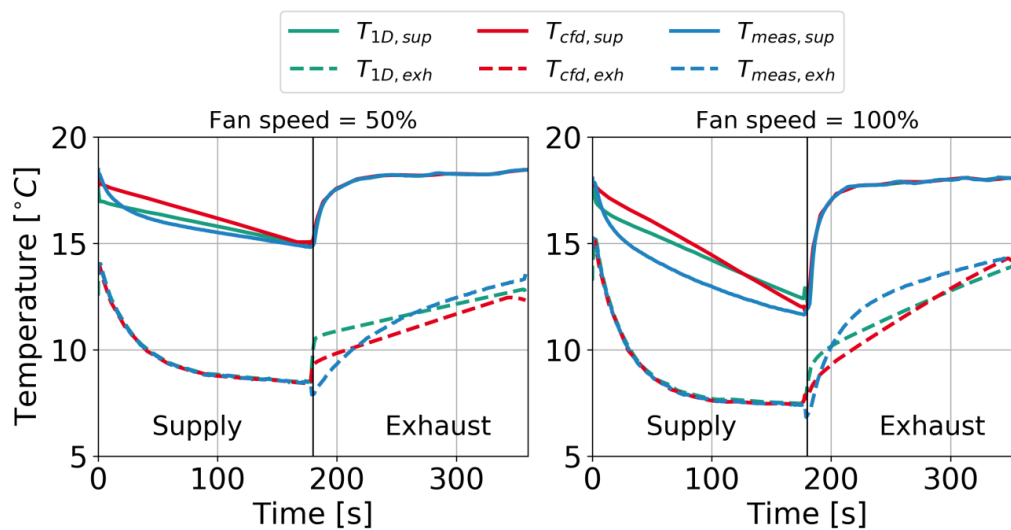


**Figure 17.** Supply and exhaust temperature comparison between both simulation models and measurements with 180 s phase.

**Table 8.** Performance indicators regarding the supply temperature for both simulation models.

Model	$T_{sup,room}$					Simulation Time
	Period (s)	60 s		180 s		
	Fan Speed	RMSE (°C)	MAPE (%)	RMSE (°C)	MAPE (%)	
CFD	50%	0.8	4.5	0.6	3.6	>8 h
	100%	1.5	9.6	1.3	9.1	
1D Model (Modelica)	50%	0.6	2.3	0.3	1.6	0.17 s
	100%	1.1	6.9	1.1	7.6	

Longer periods present lower errors, probably because the average volume flow (and, directly, the Nusselt number) is closer to the steady-state value. In other words, the volume flow uncertainty due to the direction change of the fan is proportionally shorter when the period is longer. Besides, higher fan speeds lead to higher discrepancies between measurements and simulations. The advantages of the test facility are its flexibility, size, and appropriate accuracy. This simplicity allows an increased variety of measurements. However, some limitations appeared, which resulted in a slight overestimation of the heat exchanged. A known limitation of the laboratory measurement is related to the mass flow measurement procedure. The mass flow rate in both directions (the exhaust and supply) was obtained using pressure correlations across the heat exchanger and the mean velocity. The correlations were determined in previous measurements from the same test facility with the changing position of the mass flow sensor. This was done because the mass flow sensor could only measure in one direction. Verification of the correlation validity could be carried out during cyclic measurements only in one direction. Since the fan has different characteristic curves for both directions, there is an uncertainty when applying this simplification. This could explain the lower error levels on the supply side of the regenerator and the higher error levels associated with higher fan speeds. Measurement uncertainties around the direction change in these devices have already been identified as considerable and could also affect the measurement results [13]. Other room and ambient temperature conditions can influence the obtained heat recovery efficiency, as Zemitis et al. [44] studied. Finally, there are uncertainties in the thermal properties of the regenerator, which were reported by the manufacturer.

To summarize, the key findings of this section are listed as follows:

- The 1D model sufficiently calculates the experimentally evaluated behavior of the DRVS. Longer cycles and lower air velocities are better modeled compared to the measurements.

- CFD modeling could make sense for geometrical optimization but not for cycle evaluation.
- Measured heat recovery efficiencies are in a range between 54% and 80% accuracy. Higher air velocities and shorter cycles present higher efficiencies.

This section studies the heat recovery efficiency of DRVSs in depth. There are several methods suggested by standards and scientific reports on how to calculate the heat recovery efficiency of DRVSs [19]. In this particular case, the selected one provides a simple interpretation; the efficiency indicates the reached mean supply temperature in comparison to its theoretical value, given the room and ambient temperature difference. For instance, this method, typically used by manufacturers, does not include the fan power nor the influence of air humidity. However, the influence of the mass flow rate is neglected mostly. Equation (18) assumes that the supply and exhaust mass flow rates are identical. As mentioned before, the influence of the pressure difference between the façade and the room significantly impacts the resulting airflow rates. The theoretical heat recovery potential is affected strongly by these pressure differences, especially since supply airflow rates are usually larger than exhaust ones, as Mikola et al. [6] studied. In that sense, the impact of a component-based model for the heat recovery system, as well as inclusion of a reliable hydraulic model that considers pressure difference between façade and room, must be investigated. The next section covers this point, integrating the proposed models into a building simulation case study.

#### 4. Case Study: Integrating DRVS into Building Simulation

##### 4.1. Simulation Set Up

In this section, the impact of integrating a more detailed DRVS model into a building performance simulation is analyzed and quantified. The building model was described in Section 2.5. The DRVS heat recovery model is described in Section 2.3.2, and the fan hydraulic model in Section 2.4. Three simulation case studies are carried out:

- DRVS modeling including pressure difference with a component-based HRC model.
- DRVS modeling including pressure difference with a constant HRC efficiency of 70%.
- DRVS modeling neglecting pressure difference with a constant HRC efficiency of 70%.

The simulation was performed for a full winter week (Stuttgart test reference year). The ambient temperature and wind speed for the whole simulation period are shown in Figure 18. The case that neglects the pressure difference and uses an ideal HRC efficiency is used as a baseline. The RMSE and MAPE indicators evaluate the deviations in the results of the other two simulations with the baseline case. These indicators help to create a better understanding of the differences in the variables between the different simulation scenarios. The effect on the indoor temperature is not considered since the heating system is ideal, and therefore, the indoor room temperature is fairly constant. The influence on energy consumption (heating energy losses and fan energy consumption) due to ventilation and air exchange rate are taken as indicators to evaluate this study. The direct comparison of the heating energy losses due to ventilation is possible, given that the same boundary conditions are selected in every simulation case.

##### 4.2. Simulation Results

Figure 19 shows a daily air exchange profile (in air changes per hour) of the whole dwelling due to mechanical ventilation (without infiltration or natural ventilation), with and without considering the pressure difference between the rooms and the façade. The average airflow rate in the whole dwelling is higher when considering the pressure difference, caused by modeling a constant fan speed DRVS (as usually occurs in reality), instead of a constant volume flow system. The pressure differences consider the influence of wind speed on the façade absolute pressure. In this case study, low wind speeds result in a fairly constant pressure difference between room and ambient temperatures.

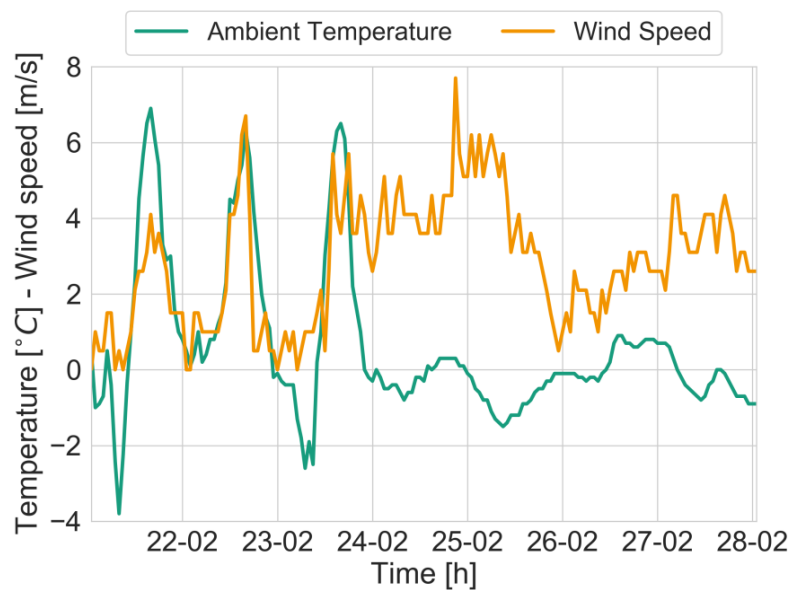


**Figure 18.** Weather conditions (ambient temperature and wind speed) during the simulation period.

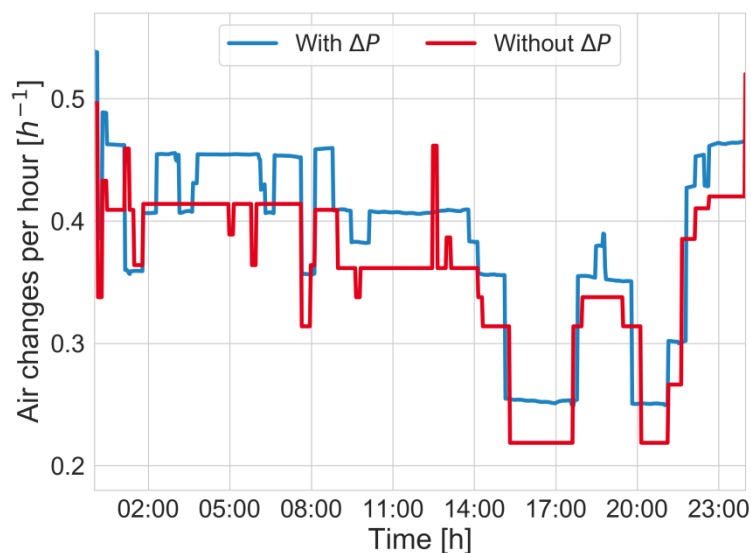


**Figure 19.** Total air exchange rate considering (with  $\Delta P$ ) and neglecting (without  $\Delta P$ ) pressure difference between the rooms and the façade in a single day.

The higher air exchange rate has an impact on energy consumption as well as in the indoor contaminant removal. In this case, differences in the  $\text{CO}_2$  concentration and relative humidity were identified between the simulation cases. In the worst-case scenario, relative differences up to 5% were seen. In this particular study, these differences could be considered negligible. However, different boundary conditions could influence the obtained results. Further discrepancies in the results between rooms with different control strategies (relative humidity or  $\text{CO}_2$ ) were not identified. As expected, rooms with a lower average air exchange rate were affected more by pressure difference, given the hydraulic modeling of the fan.

The key analysis of this section is related to energy consumption, where both pressure difference and HRC have a direct impact. Figure 20 illustrates the differences in heat losses due to ventilation and air exchange rate, relative to the simulation with ideal conditions. Component-based approaches are referred to as the “HRC Model”, in contrast to “HRC Const” (constant heat recovery efficiency). Three main findings are here identified:

- Adding the pressure difference to the fan modeling results in an 8% higher air exchange rate, which causes 9% additional heat losses. Fan energy consumption is slightly lower (−3%), as the increasing volume flows reduce the fan speed on some occasions.
- Adding a component-based heat recovery system directly impacts the heat losses due to ventilation. Relative to the constant HRC case, it results in a 17% higher total heat losses, which means that the assumption of a global heat recovery efficiency leads to an underestimation of these losses in this simulation case.
- A component-based thermal and hydraulic model of DRVS results in a total of 28% higher heat losses due to ventilation. These results are not negligible in any case and should be included when integrating DRVSs in building performance simulation.

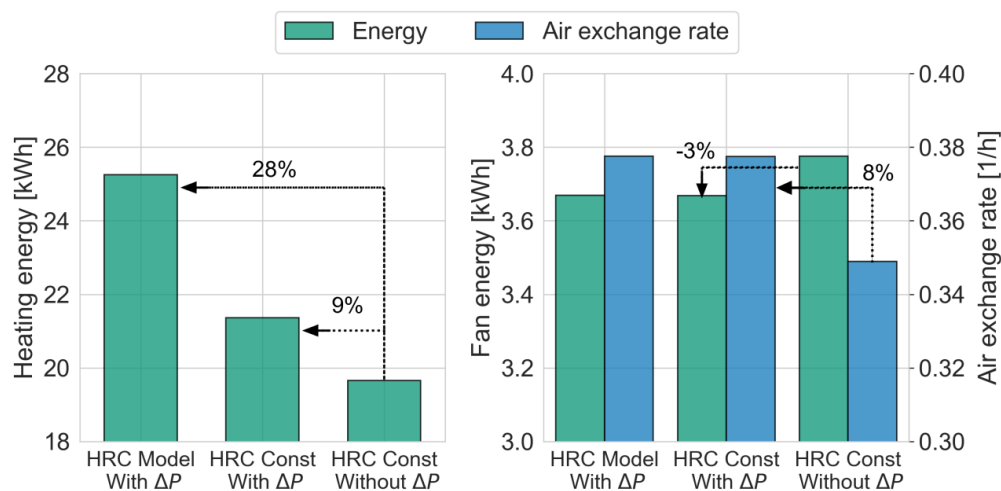


**Figure 20.** Relative increase in heat losses due to ventilation and air exchange rate for the three simulation scenarios (HRC Model = model-based; HRC Const = constant efficiency).

#### 4.3. Discussion

The results show the importance of properly modeling the DRVSs in building performance simulations. Both thermal and hydraulic modeling approaches impact the energetic performance of a building and its ventilation system. In this case, detailed modeling results in 28% higher heat losses due to ventilation and an 8% higher air exchange rate.

There are some known limitations to this study. Firstly, the selected weather file (Stuttgart, winter, test reference year) does not have a particularly high wind speed in comparison to other locations around Germany. The simulated week displays average ambient pressure and wind load profiles for this location. Selecting different simulation periods or locations may also affect the results. Higher wind loads would emphasize the influence of the pressure difference on the fan; lower fan speeds and higher air exchange rates can be expected. This confirms the approach of Baldini et al. [7], who concluded that a proper design of decentralized ventilation systems can take advantage of high wind loads to reduce the fan energy consumption. Besides, the device placement in the simulated building plays a role that is not studied in this publication (the devices were placed at the north and south façades, and in the bedroom and living room, they could be placed on the west façade). Each orientation has different wind pressure coefficients that are necessary to calculate the wind pressure in the façade [31]. Using other wind pressure coefficients will result in other pressure difference levels and, therefore, a different simulated air exchange rate in the dwelling. Furthermore, ventilation effectiveness was neglected in this study, ignoring the possibility of short-circuiting. Besides, different supply and exhaust configurations can affect the air exchange in rooms [45].

Moreover, selecting colder locations would highlight the relevance of the component-based HRC model, which confirms that considering a global heat recovery efficiency leads to an underestimation

of heating energy losses for DRVSs. Merzkirch [46] studied that increasing the heat recovery efficiency by 10% leads to a primary energy saving of 20%. Additionally, selecting different indoor temperature setpoints might affect the obtained results. The indoor temperature setpoints were taken from the DIN 1946-6 standard and are considered rather low for renovated buildings [47]. Raising those would correspondingly increase the heat losses due to ventilation, thus highlighting the importance of proper modeling of the heat recovery in DRVSs, as well as resulting in lower indoor relative humidity values.

## 5. Conclusions

Two models to simulate the heat recovery in decentralized regenerative ventilation systems (DRVS) were proposed. The first one was using CFD and the second one adopted a dynamic 1D simplification with a discretized heat storage model. Measurements were carried out in a test facility to compare the performances of both models in terms of heat recovered and course of supply and exhaust temperatures. The results showed that the CFD model has good overall performance when reproducing the heat transfer, as well as the 1D model with six nodes, which is based on a simplified approach and ignores some physical effects. The 1D model is even closer to measurements in most cases. Both models slightly overestimate the heat exchanged in supply and exhaust phases. This could be a result of inaccuracies in the mass flow measurement procedure or overestimating heat gains from the ambient or the fan. In general, both models showed an appropriate performance regarding the measured temperatures and heat exchanged (percentage errors—MAPE—under 10%). The CFD model provides a higher discretization level than the 1D model, therefore requiring much higher computational resources.

Besides, the Modelica 1D model was implemented in a building performance simulation scheme to study the influence of pressure difference and heat recovery efficiencies on the indoor environment and to evaluate the importance of a precise component-based modeling approach. The results suggest that pressure difference between a room and building façade has a strong effect on DRVSs and should not be neglected. Higher air exchange rates caused higher energy consumption and lower contaminant concentrations in the rooms. Energy is more sensitive to adequate modeling than contaminant removal. A model neglecting the effect of the pressure difference between indoors and the façade and assuming a constant heat recovery efficiency underestimates the heat losses by almost 30% and the air exchange rate by almost 10% in the simulation test case (which itself causes a 13% underestimation of the HRC efficiency).

In real situations, a potential solution to lowering the influence of wind and pressure differences between indoors and outdoors is the inclusion of volume flow control systems in these devices. This means that every ventilation level is associated with a volume flow and not with fan speed. This addition will require more sensors and advanced control algorithms to reduce the influence of wind (currently, the DCV devices have an open-loop control, associating the measured variable with a fan speed value). Another option might be to replace the axial fans in the ventilation devices with radial fans, which are less sensitive to wind pressure. Further research is foreseen to develop new DRVS technologies and optimize their control strategies by integrating models, taking into account the pressure difference in building performance simulation.

**Author Contributions:** The test facility measurements were performed by N.A. CFD and Modelica simulations were carried out by H.F. and N.C., respectively. Heat exchanger validation, building simulation, and data analysis were performed by N.C. The research conceptualization was developed by N.C., H.F., and T.P. The original draft was written by N.C., H.F., and N.A. The review and editing were performed by T.P., C.B., and L.S. Supervision was carried out by C.B. and L.S. All authors have read and agreed to the published version of the manuscript.

**Funding:** The study presented in this paper received funding from the German Federal Ministry of Economic Affairs and Energy (BMWi) under the grant agreement numbers FKZ03SBE0001B (LowEx im Bestand) and FKZ03ET1540B (HEAVEN).

**Conflicts of Interest:** The authors declare no conflict of interest. The funders had no role in the design of the study; in the collection, analyses, or interpretation of data; in the writing of the manuscript, or in the decision to publish the results.

## Nomenclature

### Variables

$Q$	Heat exchanged
$\dot{Q}$	Heat transfer rate
$\Delta P$	Pressure difference
$\dot{V}$	Volume flow
$\eta$	Efficiency
$P$	Power
$T$	Temperature
$t$	Time
$\dot{m}$	Mass flow
$c_p$	specific heat coefficient
$Nu$	Nusselt number
$Re$	Reynolds number
$Pr$	Prandtl number
$n_{\text{chan}}$	Number of channels
$w$	Channel width
$l$	Channel length
$\rho$	Density
$k$	Thermal conductivity
$t_{\text{wall}}$	Wall thickness
$A$	Area
$h$	Specific convection coefficient
$d_h$	Hydraulic diameter

### Subscripts

meas	Measured
1D	Simulated with 1D model
cfD	Simulated with CFD model
mean	Mean value
room	Room or indoor side
amb	Ambient or outdoor side
sup	Supply
exh	Exhaust
air	Air stream
solid	Regenerator
inf	Infiltrations
ht	Heat transfer
flow	Flowing

### Abbreviations

BDF	Backward differentiation formula
CFD	Computational fluid dynamics
DRVS	Decentralized regenerative ventilation system
DCV	Demand controlled ventilation
FEM	Finite elements method
GCI	Grid convergence indices
HRC	Heat recovery
MAPE	Mean absolute percentage error
RMSE	Root mean squared error

## References

1. European Union Commission. *Comprehensive Study of Building Energy Renovation Activities and the Uptake of Nearly Zero-Energy Buildings in the EU*; European Commission: Brussels, Belgium, 2019; Available online: <https://op.europa.eu/de/publication-detail/-/publication/97d6a4ca-5847-11ea-8b81-01aa75ed71a1> (accessed on 20 July 2020).
2. Francisco, P.W.; Jacobs, D.E.; Targos, L.; Dixon, S.L.; Breyse, J.; Rose, W.; Cali, S. Ventilation, indoor air quality, and health in homes undergoing weatherization. *Indoor Air* **2017**, *27*, 463–477. [[CrossRef](#)] [[PubMed](#)]
3. Interconnection Consulting. *IC Market Tracking: Kontrollierte Wohnraumlüftung in Europa 2018*; Interconnection Consulting: Oberstdorf, Germany, 2018; Available online: [www.interconnectionconsulting.com](http://www.interconnectionconsulting.com) (accessed on 14 October 2019).
4. Viessmann GbmH. Dezentrales Wohnungslüftungsgerät Vitovent 100-D mit Wärmerückgewinnung. Available online: <https://www.viessmann.de/de/wohngebaeude/wohnungslueftung/dezentrale-wohnungslueftung/vitovent-100-d.html> (accessed on 20 July 2020).
5. Angsten, R.; Hartmann, T. Raumweise Lüftungsgeräte in der Wohnungslüftung—Pro und contra. *GI Wiss.* **2017**, *3*, 210–215.
6. Mikola, A.; Simson, R.; Kurnitski, J. The Impact of Air Pressure Conditions on the Performance of Single Room Ventilation Units in Multi-Story Buildings. *Energies* **2019**, *12*, 2633. [[CrossRef](#)]
7. Baldini, L.; Goffin, P.; Leibundgut, H. Control strategies for effective use of wind loading through a decentralized ventilation system. In Proceedings of the ROOMVENT 2011-12th International Conference on Air Distribution in Rooms, Trondheim, Norway, 10–12 January 2021.
8. Mahler, B.; Himmler, R. Results of the evaluation study DeAL Decentralized facade integrated ventilation systems. In Proceedings of the 8th International Conference for Enhanced Building Operations, Berlin, Germany, 20–22 October 2008; pp. 1–8.
9. Merzkirch, A.; Maas, S.; Scholzen, F.; Waldmann, D. Field tests of centralized and decentralized ventilation units in residential buildings—Specific fan power, heat recovery efficiency, shortcuts and volume flow unbalances. *Energy Build.* **2016**, *116*, 376–383. [[CrossRef](#)]
10. Coydon, F.; Herkel, S.; Kuber, T.; Pfaffertott, J.; Himmelsbach, S. Energy performance of façade integrated decentralised ventilation systems. *Energy Build.* **2015**, *107*, 172–180. [[CrossRef](#)]
11. Smith, K.; Svendsen, S. Control of Single-room Ventilation with Regenerative Heat Recovery for Indoor Climate and Energy Performance. In Proceedings of the CLIMA 2016—12th REHVA World Congress, Aalborg, Denmark, 22–25 May 2016.
12. Manz, H.; Huber, H.; Schälín, A.; Weber, A.; Ferrazzini, M.; Studer, M. Performance of single room ventilation units with recuperative or regenerative heat recovery. *Energy Build.* **2000**, *31*, 37–47. [[CrossRef](#)]
13. Mathis, P.; Röder, T.; Hartmann, T.; Knaus, C.; Klein, B.; Müller, D. Ventilation efficiency of decentralized alternating residential ventilation unit. *REHVA J.* **2019**, *4*, 8–12.
14. Muralikrishna, S. Study of Heat Transfer Process in a Regenerator. *Chem. Eng. Res. Des.* **1999**, *77*, 131–137. [[CrossRef](#)]
15. Liu, H.; Yu, Q.N.; Zhang, Z.C.; Qu, Z.G.; Wang, C.Z. Two-equation method for heat transfer efficiency in metal honeycombs: An analytical solution. *Int. J. Heat Mass Transf.* **2016**, *97*, 201–210. [[CrossRef](#)]
16. Mesonero, I.; Febres, J.; López Pérez, S. Modeling and simulation of fixed bed regenerators for a multi-tower decoupled advanced solar combined cycle. In Proceedings of the 12th International Modelica Conference, Prague, Czech Republic, 15–17 May 2017; pp. 847–855. [[CrossRef](#)]
17. Gateau, P.; Namy, P.; Huc, N. Comparison between Honeycomb and Fin Heat Exchangers. In Proceedings of the Comsol Conference. 2011. Available online: <https://www.tib.eu/en/search/id/TIBKAT%3A689211589/> (accessed on 31 December 2012).
18. Li, Q.; Wang, Z.; Bai, F.; Chu, S.; Yang, B. Thermal Analysis of Honeycomb Ceramic Air Receiver. In *AIP Conference Proceedings 1850*; AIP Publishing LLC: Melville, NY, USA, 2017; Volume 160016. [[CrossRef](#)]
19. Auerswald, S.; Pflug, T.; Engelmann, P.; Carbonare, N.; Bongs, C.; Dinkel, A.; Henning, H.-M. A holistic evaluation method for decentralized ventilation systems. In Proceedings of the 39th AIVC Conference, Antibes Juan-Les-Pins, France, 18–19 September 2018.

20. Ljubijankic, M.; Nytsch-Geusen, C.; Rädler, J.; Löffler, M. Numerical coupling of Modelica and CFD for building energy supply systems. In Proceedings of the 8th Modelica Conference, Dresden, Germany, 20–22 March 2011; pp. 286–294.
21. Asadov, N. Simulation and Measurement of Different Geometries and Materials for Heat Exchangers in Decentralized Regenerative Ventilation Devices. Master's Thesis, Fraunhofer ISE, Universität Freiburg, Freiburg im Breisgau, Germany, 2019.
22. Celik, I.B.; Ghia, U.; Roache, P.J.; Freitas, C.J.; Coleman, H.; Raad, P.E. Procedure for Estimation and Reporting of Uncertainty Due to Discretization in CFD Applications. *J. Fluids Eng.* **2008**, *130*. [CrossRef]
23. Li, Q.; Bai, F.; Yang, B.; Wang, Z.; El Hefni, B.; Liu, S.; Kubo, S.; Kiriki, H.; Han, M. Dynamic simulation and experimental validation of an open air receiver and a thermal energy storage system for solar thermal power plant. *Appl. Energy* **2016**, *178*, 281–293. [CrossRef]
24. Shah, R.K.; Sekulić, D.P. *Fundamentals of Heat Exchanger Design*; John Wiley & Sons: Hoboken, NJ, USA, 2003; ISBN 0471321710.
25. Mattsson, S.E.; Elmqvist, H. Modelica—An international effort to design the next generation modeling language. In Proceedings of the 7th IFAC Symposium on Computer Aided Control Systems Design, Gent, Belgium, 28–30 April 1997; pp. 1–5.
26. Wetter, M.; Zuo, W.; Nouidui, T.S.; Pang, X. Modelica Buildings library. *J. Build. Perform. Simul.* **2014**, *7*, 253–270. [CrossRef]
27. Deutsches Institut für Bautechnik. *Zulassungsbericht Z-51.3-415: Dezentrales Wohnungslueftungsgeraet mit Waermerueckgewinnung vom Typ Vitovent 100-D H00E A45*; DIBt: Berlin, Germany, 2019.
28. Ebert, B. LowEx-Bestand Analyse Abschlussbericht zu AP 1.1. Systematische Analyse von Mehrfamilien-Bestandsgebäuden. 2018. Available online: <https://www.lowex-bestand.de/index.php/downloads/?lang=de&download=77> (accessed on 20 March 2019).
29. Crawley, D.B.; Lawrie, L.K.; Winkelmann, F.C.; Buhl, W.F.; Huang, Y.J.; Pedersen, C.O.; Strand, R.K.; Liesen, R.J.; Fisher, D.E.; Witte, M.J.; et al. EnergyPlus: Creating a new-generation building energy simulation program. *Energy Build.* **2001**, *33*, 319–331. [CrossRef]
30. Boyer, H.; Lauret, A.P.; Adelard, L.; Mara, T.A. Building ventilation: A pressure airflow model computer generation and elements of validation. *Energy Build.* **1999**, *29*, 283–292. [CrossRef]
31. Swami, M.V.; Chandra, S. *Procedures for Calculating Natural Ventilation Airflow Rates in Buildings*; ASHRAE Research Project 448-RP No. 1; Florida Solar Energy Center: Cocoa, FL, USA, 1987.
32. Orme, M.; Liddament, M.W.; Wilson, A. *Numerical Data for Air Infiltration & Natural Ventilation Calculation*; Energy Conservation in buildings and Community Systems Program; AIVC: Coventry, UK, February 1998.
33. International Organization for Standardization. *ISO 18523-2:2018—Energy Performance of Buildings—Schedule and Condition of Building—Zone and Space Usage for Energy Calculation. Part 2: Residential Buildings*, 1st ed.; ISO: Geneva, Switzerland, 2018.
34. Ahmed, K.; Kurnitski, J.; Olesen, B. Data for occupancy internal heat gain calculation in main building categories. *Data Brief* **2017**, *15*, 1030–1034. [CrossRef]
35. Firlag, S.; Zawada, B. Impacts of airflows, internal heat and moisture gains on accuracy of modeling energy consumption and indoor parameters in passive building. *Energy Build.* **2013**, *64*, 372–383. [CrossRef]
36. TenWolde, A.; Pilon, C.L. The Effect of Indoor Humidity on Water Vapor Release in Homes. In *Proceedings Thermal Performance of the Exterior Envelopes of 2007*; Building: Clearwater, FL, USA, 2007.
37. Persily, A.; de Jonge, L. Carbon dioxide generation rates for building occupants. *Indoor Air* **2017**, *27*, 868–879. [CrossRef]
38. Schweiker, M.; Haldi, F.; Shukuya, M.; Robinson, D. Verification of stochastic models of window opening behaviour for residential buildings. *J. Build. Perform. Simul.* **2012**, *5*, 55–74. [CrossRef]
39. Deutsches Institut für Normung e.V. *DIN 1946-6-Raumlufttechnik- Teil 6-Lüftung von Wohnungen—Allgemeine Anforderungen, Anforderungen an die Auslegung, Ausführung, Inbetriebnahme und Übergabe sowie Instandhaltung*, 1st ed.; Beuth Verlag GmbH: Berlin, Germany, 2019.
40. Carbonare, N.; Pflug, T.; Bongs, C.; Wagner, A. Comfort-oriented control strategies for decentralized ventilation using co-simulation. *IOP Conf. Ser. Mater. Sci. Eng.* **2019**, *609*, 1–6. [CrossRef]
41. Carbonare, N.; Pflug, T.; Bongs, C.; Wagner, A. Simulation study of a novel fuzzy demand controlled ventilation for façade-integrated decentralized systems. *Sci. Technol. Built Environ.* **2020**, *26*, 1412–1426. [CrossRef]



42. Deutsches Institut für Normung e.V.; European Committee for Standardization. *DIN EN 308. Wärmeaustauscher—Prüfverfahren zur Bestimmung der Leistungskriterien von Luft/Luft und Luft/Abgas-Wärmerückgewinnungsanlagen*; Beuth Verlag GmbH: Berlin, Germany, 1997.
43. Armstrong, J.S.; Collopy, F. Error measures for generalizing about forecasting methods: Empirical comparisons. *Int. J. Forecast.* **1992**, *8*, 69–80. [[CrossRef](#)]
44. Zemitis, J.; Bogdanovics, R. Heat recovery efficiency of local decentralized ventilation device at various pressure differences. *Mag. Civil Eng.* **2020**, *94*, 120–128. [[CrossRef](#)]
45. Krajčík, M.; Simone, A.; Olesen, B.W. Air distribution and ventilation effectiveness in an occupied room heated by warm air. *Energy Build.* **2012**, *55*, 94–101. [[CrossRef](#)]
46. Merzkirch, A. Energieeffizienz, Nutzerkomfort und Kostenanalyse von Lüftungsanlagen in Wohngebäuden: Feldtests von neuen Anlagen und Vorstellung bedarfsgeführter Prototypen. Ph.D. Thesis, Université du Luxembourg, Luxembourg, 2015.
47. Pastore, L.; Andersen, M. Building energy certification versus user satisfaction with the indoor environment: Findings from a multi-site post-occupancy evaluation (POE) in Switzerland. *Build. Environ.* **2019**, *150*, 60–74. [[CrossRef](#)]

**Publisher's Note:** MDPI stays neutral with regard to jurisdictional claims in published maps and institutional affiliations.



© 2020 by the authors. Licensee MDPI, Basel, Switzerland. This article is an open access article distributed under the terms and conditions of the Creative Commons Attribution (CC BY) license (<http://creativecommons.org/licenses/by/4.0/>).